

First Measurement of a Long-Lived $\pi^+\pi^-$ Atom Lifetime

B. Adeva,¹ L. Afanasyev,² A. Anania,³ S. Aogaki,⁴ A. Benelli,⁷ V. Brekhovskikh,⁶ T. Cechak,⁷ M. Chiba,⁸ P. V. Chliapnikov,⁶ P. Doskarova,⁷ D. Drijard,⁹ A. Dudarev,² D. Dumitriu,⁴ D. Fluerasu,⁴ A. Gorin,⁶ O. Gorchakov,^{2,†} K. Gritsay,² C. Guaraldo,¹⁰ M. Gugiu,⁴ M. Hansroul,⁹ Z. Hons,¹¹ S. Horikawa,⁵ Y. Iwashita,¹² V. Karpukhin,² J. Kluson,⁷ M. Kobayashi,¹³ V. Kruglov,² L. Kruglova,² A. Kulikov,² E. Kulish,² A. Lamberto,³ A. Lanaro,^{9,14} R. Lednicky,¹⁵ C. Mariñas,¹ J. Martincik,⁷ L. Nemenov,^{2,9} M. Nikitin,² K. Okada,¹⁶ V. Olchevskii,² V. Ovsiannikov,¹⁷ M. Pentia,⁴ A. Penzo,¹⁸ M. Plo,¹ P. Prusa,⁷ G. F. Rappazzo,³ A. Romero Vidal,¹ A. Ryazantsev,⁶ V. Rykalin,⁶ J. Saborido,¹ J. Schacher,^{19,*} A. Sidorov,⁶ J. Smolik,⁷ F. Takeutchi,¹⁶ T. Trojek,⁷ S. Trusov,²⁰ T. Urban,⁷ T. Vrba,⁷ V. Yazkov,^{20,†} Y. Yoshimura,¹³ and P. Zrelov²

¹Santiago de Compostela University, Santiago de Compostela, Spain

²JINR, Dubna, Russia

³INFN, Sezione di Trieste and Messina University, Messina, Italy

⁴IFIN-HH, National Institute for Physics and Nuclear Engineering, Bucharest, Romania

⁵Zurich University, Zurich, Switzerland

⁶IHEP, Protvino, Russia

⁷Czech Technical University in Prague, Prague, Czech Republic

⁸Tokyo Metropolitan University, Tokyo, Japan

⁹CERN, Geneva, Switzerland

¹⁰INFN, Laboratori Nazionali di Frascati, Frascati, Italy

¹¹Nuclear Physics Institute ASCR, Rez, Czech Republic

¹²Kyoto University, Kyoto, Japan

¹³KEK, Tsukuba, Japan

¹⁴University of Wisconsin, Madison, Wisconsin USA

¹⁵Institute of Physics ASCR, Prague, Czech Republic

¹⁶Kyoto Sangyo University, Kyoto, Japan

¹⁷Voronezh State University, Voronezh, Russia

¹⁸INFN, Sezione di Trieste, Trieste, Italy

¹⁹Albert Einstein Center for Fundamental Physics, LHEP, Bern, Switzerland

²⁰Skobeltsin Institute for Nuclear Physics of Moscow State University, Moscow, Russia



(Received 29 November 2018; published 1 March 2019)

The adapted DIRAC experiment at the CERN PS accelerator observed for the first time long-lived hydrogenlike $\pi^+\pi^-$ atoms, produced by protons hitting a beryllium target. A part of these atoms crossed the gap of 96 mm between the target and a 2.1 μm thick platinum foil, in which most of them dissociated. Analyzing the observed number of atomic pairs, $n_A^L = 436_{-61}^{+157}|_{\text{tot}}$, the lifetime of the $2p$ state is found to be $\tau_{2p} = (0.45_{-0.30}^{+1.08}|_{\text{tot}}) \times 10^{-11}$ s, not contradicting the corresponding QED $2p$ state lifetime $\tau_{2p}^{\text{QED}} = 1.17 \times 10^{-11}$ s. This lifetime value is three orders of magnitude larger than our previously measured value of the $\pi^+\pi^-$ atom ground state lifetime $\tau = (3.15_{-0.26}^{+0.28}|_{\text{tot}}) \times 10^{-15}$ s. Further studies of long-lived $\pi^+\pi^-$ atoms will allow us to measure energy differences between p and s atomic states and so to discriminate between the isoscalar and isotensor $\pi\pi$ scattering lengths with the aim to check QCD predictions.

DOI: 10.1103/PhysRevLett.122.082003

Introduction.—The DIRAC collaboration aims to check low-energy QCD predictions using double-exotic $\pi^+\pi^-$

and $\pi^\pm K^\mp$ atoms, which have been observed and studied [1–7]. In strong inclusive processes, these atoms are produced in s states and are distributed according to n^{-3} , n being the principal quantum number [8].

The decay probability of short-lived $\pi^+\pi^-$ atoms ($A_{2\pi}$, pionium) in s states is dominated (99.6%) by the annihilation process [9–13] $\pi^+ + \pi^- \rightarrow \pi^0 + \pi^0$ and is given by the $\pi\pi$ s -wave scattering lengths combination $|a_0 - a_2|$ (a_I is the $\pi\pi$ scattering length for isospin I):

Published by the American Physical Society under the terms of the Creative Commons Attribution 4.0 International license. Further distribution of this work must maintain attribution to the author(s) and the published article's title, journal citation, and DOI. Funded by SCOAP³.

$$\frac{1}{\tau} \approx \Gamma(A_{2\pi} \rightarrow \pi^0 \pi^0) = R |a_0 - a_2|^2 \quad \text{with} \quad R \propto |\psi_{nl}(0)|^2. \quad (1)$$

The expression $\psi_{nl}(0)$ is the pure Coulomb atomic wave function at the origin with principal quantum number n and orbital quantum number l . The correction to Eq. (1) concerning finite pion size is negligible. The precision of the ratio R is 1.2% [13], and the scattering lengths and their combination have been calculated in low-energy QCD [14]. The DIRAC experiment has measured such lifetimes and so derived combined $\pi\pi$ [1–3] and for the first time πK [5,7] scattering lengths.

After investigation of $\pi\pi$ and πK atoms with “short” lifetimes of order 10^{-15} s, DIRAC continues to study $\pi\pi$ atomic states ($A_{2\pi}^L$) of “long” lifetimes of order 10^{-11} s as considered in Ref. [8]. Moving inside the target, relativistic short-lived $A_{2\pi}$ interact with the electric field of the target atoms, resulting in a possible change of the $A_{2\pi}$ orbital momentum l by one or more units. Some (N_A^l) of them (N_A) will leave the target with $l > 0$. For such states, $|\psi_{nl}(0)|^2 = 0$ and thus all decays are suppressed in accordance with Eq. (1). Therefore, the decay mechanism of such excited states is the radiative de-excitation to an ns state, annihilating subsequently with the “short” lifetime τn^3 into two π^0 . The shortest $A_{2\pi}^L$ lifetime is the $2p$ state lifetime $\tau_{2p} \approx \tau_{2p}^{\text{QED}} = 1.17 \times 10^{-11}$ s [8,15], which is more than three orders of magnitude larger than the minimum $A_{2\pi}$ lifetime. For an average momentum of detected $A_{2\pi}$ $\langle p_A \rangle = 4.44$ GeV/ c ($\gamma \simeq 15.9$), the decay lengths are 5.6 cm ($2p$), 18.4 cm ($3p$), 43 cm ($4p$), 83 cm ($5p$), and 143 cm ($6p$).

These large atom decay lengths in the laboratory (lab) system open a possibility to measure the energy splitting between ns and np levels. This splitting is given by the precisely calculated QED Lamb shift and the hadronic ns level shift, which depends on a different combination of $\pi\pi$ scattering lengths, $2a_0 + a_2$ [16,17].

In this Letter, the DIRAC collaboration presents the first lifetime measurement of long-lived $\pi^+\pi^-$ atoms, observed by DIRAC as described in Ref. [18].

Setup for investigation of long-lived $\pi^+\pi^-$ atoms.—To investigate long-lived $A_{2\pi}^L$ atoms, the primary 24 GeV/ c CERN PS proton beam with intensity of 3.0×10^{11} protons per spill [19] hits a 103 μm thick Be target (Figs. 1 and 2). On their way to the 2.1 μm thick Pt foil at a distance of 96 mm behind the Be target, a part of the produced long-lived atoms $A_{2\pi}^L$, depending on their lifetimes, decays, whereas the other part enters the Pt foil. By interacting with Pt atoms, the atoms $A_{2\pi}^L$ break up (get ionized) and generate atomic $\pi^+\pi^-$ pairs with relative momenta $Q < 3$ MeV/ c in their pair center-of-mass (c.m.) system. The foil is introduced at 7.5 mm above the primary proton beam to avoid interaction of the beam halo with Pt. The beam position in

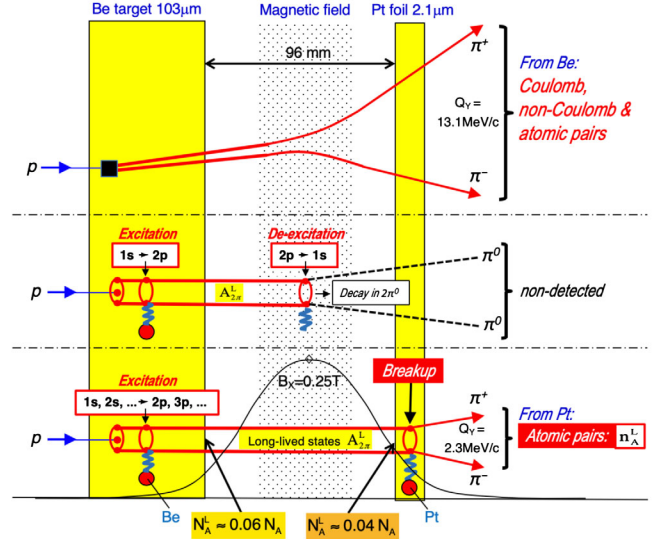


FIG. 1. Method to investigate long-lived $A_{2\pi}^L$ by means of a breakup foil (side view). N_A is the number of the totally produced $A_{2\pi}^L$ and N_A^l the number of excited $A_{2\pi}^L$ with $l > 0$.

the vertical plane was permanently monitored. Between target and breakup foil, there was installed a permanent retractable magnet [20] with a pole distance of 60 mm (insertion of Fig. 2) and a maximum horizontal field strength of 0.25 T (bending power 0.02 Tm). The magnet enlarges the value of the vertical component Q_Y of $\pi^+\pi^-$ pairs, generated in Be, on $Q_Y = 13.15$ MeV/ c (see Fig. 1). For simulated events, this value is $Q_Y = 13.12$ MeV/ c . For all pairs generated in Pt foil, the fringing magnetic field modifies the vertical component Q_Y only by 2.3 MeV/ c . This large difference in the Q_Y shift for pairs from Be and Pt allows us to suppress the background by a factor of about

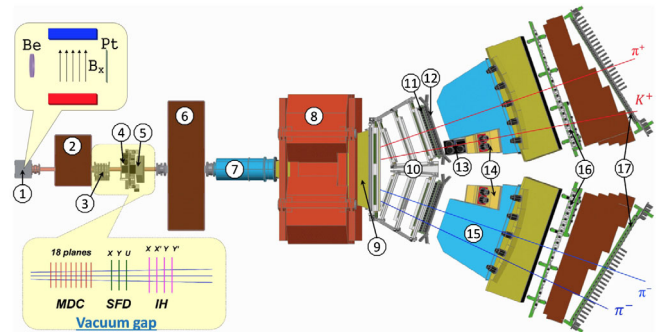


FIG. 2. Top view of the DIRAC setup: 1—target station with insertion, showing the Be target, magnetic field, and Pt breakup foil; 2—first shielding; 3—microdrift chambers (MDC); 4—scintillating fiber detector (SFD); 5—ionization hodoscope (IH); 6—second shielding; 7—vacuum tube; 8—spectrometer magnet; 9—vacuum chamber; 10—drift chambers (DC); 11—vertical hodoscope (VH); 12—horizontal hodoscope (HH); 13—aerogel Cherenkov; 14—heavy gas Cherenkov; 15—nitrogen Cherenkov; 16—preshower (PSh); 17—muon detector. (The plotted symmetric and asymmetric events are a $\pi\pi$ and πK pair, respectively.)

6 in detecting atomic pairs from long-lived $A_{2\pi}^L$. For e^+e^- pairs generated in Be, the peak is shifted to $Q_Y = 12.9$ MeV/c and its position used to measure the magnetic field stability during the six-month data taking [18].

The DIRAC setup [21], sketched in Fig. 2, identifies pions, kaons, protons, electrons, and muons by means of Cherenkov, preshower and muon detectors, and time-of-flight measurement. The achieved resolution in the particle momentum is $\Delta p/p \simeq 3 \times 10^{-3}$ and the precision of the Q components $\sigma_{QX} \approx \sigma_{QY} \approx 0.44$ MeV/c and $\sigma_{QL} \approx 0.50$ MeV/c. This high resolution enables the extraction of an atom signal in form of small Q atomic pairs. The secondary channel with the solid angle $\Omega = 1.2 \times 10^{-3}$ sr is vertically inclined relative to the proton beam by 5.7° upward.

The events are reconstructed by means of the DIRAC $\pi\pi$ analysis software described in Ref. [18], exploiting information from DC, SFD, IH, and the proton beam position on the target. The setup is aligned using properties of Λ ($\bar{\Lambda}$) decays [22].

Generation of short-lived $\pi^+\pi^-$ atoms, Coulomb, and non-Coulomb pairs.—Coulomb $\pi^+\pi^-$ pairs are produced either directly or originate from short-lived (e.g., Δ , ρ) or medium-lived (e.g., ω , ϕ) particles. These pairs undergo Coulomb final state interaction (FSI), resulting in modified unbound states or atoms. Pairs from long-lived sources (e.g., η' , η), called non-Coulomb, are nearly unaffected by Coulomb interaction. The accidental pairs arise from different interactions.

The cross section of $\pi^+\pi^-$ atom production is expressed via the inclusive production cross section of $\pi^+\pi^-$ pairs from short-lived sources without FSI, multiplied by $|\psi_{nl}(0)|^2$ [8]. The latter factor differs from zero only for s states. Thus, atoms are only produced in s states with probabilities dictated by the n dependence of $|\psi_{nl}(0)|^2$ as n^{-3} : $W_1 = 83.2\%$, $W_2 = 10.4\%$, $W_3 = 3.1\%$, $W_{n>3} = 3.3\%$.

In complete analogy, the production of $\pi^+\pi^-$ Coulomb pairs is expressed via the inclusive production cross section of $\pi^+\pi^-$ pairs without FSI, modified by the Coulomb enhancement function $A_C(q)$, which depends on the pair relative momentum q ($\sim 1/q$ for small q). This function, the well-known Gamov-Sommerfeld-Sakharov factor [23–25], is used for simulation of Coulomb pairs.

The relative yield between atoms and Coulomb pairs [26] is expressed by the ratio of the above cross sections. Thus, the total number N_A of produced $A_{2\pi}$ is determined via the number of Coulomb pairs N_C by the model-independent relation:

$$N_A = K(q_0)N_C(q \leq q_0) \quad \text{with} \quad K(2 \text{ MeV}/c) = 0.615, \quad (2)$$

where $N_C(q \leq q_0)$ is the number of Coulomb pairs with $q \leq q_0$ and $K(q_0)$ a known function of q_0 [26].

Production of long-lived $\pi^+\pi^-$ atoms.—The short-lived $\pi^+\pi^-$ atoms, which propagate in the Be target after their

production in ns states, are either decaying or interacting with Be. This interaction with the electric field of target atoms will excite or deexcite or break up $\pi^+\pi^-$ atoms. In the excitation or deexcitation processes, the orbital momentum is changed by one unit or more, so forming long-lived atoms. The lifetime of $\pi^+\pi^-$ atoms in the lab system depends on the quantum numbers n , l , and the atom momentum.

The populations of all atomic states with quantum numbers n , l , and m , as a multilevel quantum system, are described by an infinite set of transport equations in terms of probabilities [27,28]. These equations account for excitation or deexcitation and annihilation processes and describe the atomic state populations from the production point up to the target exit. For the calculations below, we use our measured value of the $A_{2\pi}$ ground state lifetime $\tau = 3.15 \times 10^{-15}$ s [3] and the spectrum of the atom lab momentum in the range 3–8 GeV/c with the average atom momentum $\langle p_A \rangle = 4.44$ GeV/c, extracted from the experimental distribution of the Coulomb pairs.

Population of long-lived states: In this Letter, the transport equations are solved numerically for all states with principal quantum numbers $n \leq 10$. The populations of states with higher n are taken into account by an extrapolation procedure. Only total, excitation and deexcitation cross sections are considered: the cross sections are calculated in the first Born approximation (one-photon exchange), using Molière parametrization of the Thomas-Fermi form factors for Be and Pt atoms.

Figure 3 shows the atomic state population P_n^L versus n , summed over l and m , at the exit of the Be target and before the Pt foil. The almost pure exponential behavior at high n allows us to extrapolate to $n > 10$ and to evaluate the population of the non-negligible infinite “tail.” Thus, the population of all discrete states can be estimated. The population at $n = 10$ is excluded from the extrapolation procedure, as this population is underestimated because of cutting the infinite set of transport equations, excluding deexcitations to this state from higher n states. The cut

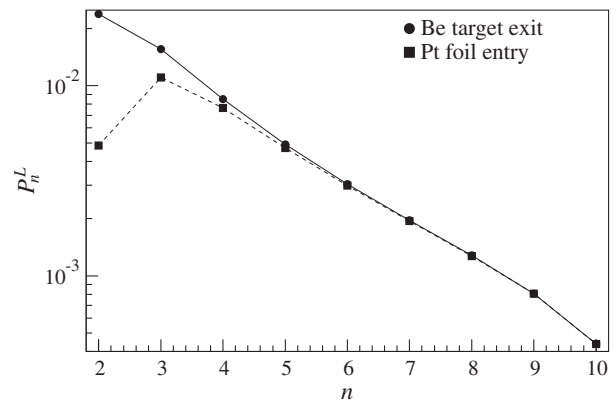


FIG. 3. Populations P_n^L of long-lived states $A_{2\pi}^L$ versus n , summed over l and m , at the exit of the Be target (filled circle) and at the Pt foil entry (filled square).

influence on the level populations is rapidly decreasing with decreasing n , as $\Delta n = 1$ transitions dominate. A fitting procedure over all points is badly suited for the “tail” estimation, as the n dependence is mainly dictated by two different dependences: production rates as n^{-3} and total cross sections roughly as n^2 . The following two n dependences are chosen for extrapolation: exponential, $a \exp(-bn)$, and hyperbolic, $cn^{-3} + dn^{-5}$. The free parameters a , b and c , d have been calculated for n , using the populations P_n^L and P_{n-1}^L .

Figure 4 illustrates the “tail” estimations. The numerical solution of the transport equations are obtained for $n \leq 10$. Then, the populations at $n = 9$ and 8 are used for the “tail” estimation. The two upper points at $n = 9$ in Fig. 4 show the sum of the populations for $n \leq 9$ plus the different “tail” estimations (exponential—filled circle, hyperbolic—filled triangle). The lower point (filled square) presents the sum of the populations with $n \leq 9$ plus the population for $n = 10$ instead of the “tail.” The curves are obtained by applying the same procedure to the points with lower n . The exponential “tail” estimation is chosen as the mean value for the population of long-lived states, as it has the smallest slope and is nearly flat for $n \geq 7$. The two other curves are used as error band.

The following numerical values are calculated: the sum of the long-lived state population at the Be exit is 6.04% for $n \leq 10$ (5.99% for $n \leq 9$) of the total number N_A of produced $A_{2\pi}$; the exponential “tail” $n \geq 10$ is 0.14%, the hyperbolic “tail” 0.25%, and the population of all long-lived states at the Be exit is given as $N_A^{L,Be} = (6.13_{-0.09}^{+0.11}) \times 10^{-2} \times N_A$. Let us underline that the accuracy of all above numbers accounts only for the precision of the extrapolation procedure.

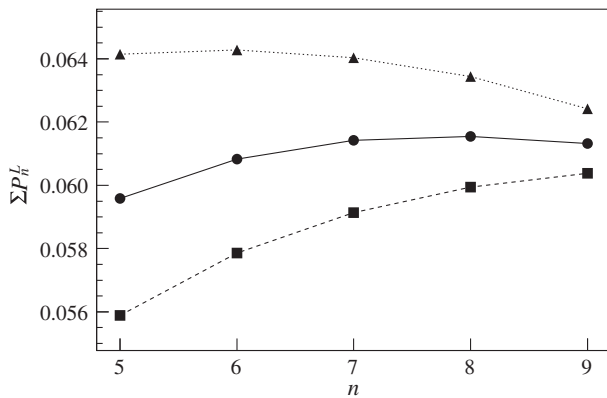


FIG. 4. Summed populations $\sum P_n^L$ of all long-lived atomic states at the exit of the Be target as a function of n used for “tail” estimation. For each n , the two upper curves show the sum of state populations for the given n plus different “tail” estimations calculated from populations for n and $n - 1$ (exponential “tail”—filled circle, hyperbolic “tail”—filled triangle). The lower curve (filled square) presents the sum of the population for the given n plus the population for $n + 1$ instead of the “tail.”

As mentioned above, the cut of the infinite set of transport equations at $n \leq 10$ leads to a small underestimation of all low-lying states because of neglecting the deexcitation from the truncated “tail” with $n > 10$. A possible influence of this cut has been estimated by comparing the above solution with a solution, cut at $n \leq 9$, where the deexcitation from states with $n = 10$ are also truncated. Estimated in this way, the population of long-lived states at the Be exit is with a very conservatively chosen error band $(6.29_{-0.13}^{+0.33}) \times 10^{-2}$ [29].

An additional correction to this value may arise from the accuracy of atom-atom cross sections. In the case of the Be target, an estimation shows that the summed population of long-lived states for $n \leq 8$ at the Be exit, calculated with the most accurate cross sections [30–32], is 2.8% less than the current value. Thus, this value can be used as the scale factor accounting for uncertainties of the used atom-atom cross sections. Further, the accuracy of the most accurate cross sections is estimated to be about 1% [30–32], which can be converted roughly to a 1% error in the populations. Let us conservatively add this error linearly to the latter error band. Finally, the population of long-lived states at the Be exit is $(6.12_{-0.19}^{+0.39}) \times 10^{-2}$, compared to $(6.13_{-0.09}^{+0.11}) \times 10^{-2}$ in the above calculations. Thus, this crude accuracy estimation leads mainly to an increase of the error band for the calculated probabilities. Nevertheless, it is significantly smaller than the experimental error. Hence, its influence is applied only to the final results as described below.

Decay in gap and breakup in Pt for long-lived atoms: In the 96 mm gap between the Be target and the Pt foil, the populations of the atomic states alter depending on their lifetime [15], calculated in QED. The decay length of atoms with fixed n is minimal for $l = 1$ and strongly increasing with l . Figure 3 indicates that mainly states with $n = 2-4$ are decaying in the gap. The summed population of long-lived states at the entry of the Pt foil is 0.037 ± 0.001 . Note that all cascade radiation transitions between atomic states as well as annihilation of ns states are considered, using the technique of transport equations. The cascade accounting increases the summed population by about 10% compared to a pure exponential decay.

Table I shows the summed populations of long-lived states at the Be target exit and at the Pt foil entry as a function of n . Illustrative values of np state breakup probabilities in the Pt foil are shown as well. The pionium breakup in Pt is treated in the same way as the breakup in the target. The breakup probability of $A_{2\pi}^L$ entering in Pt, averaged over populations, is 0.944.

Finally, the expected total probability $P_{br}^{tot}(Pt)$, that pionium produced in Be will break up in Pt, is calculated via the difference between the total populations at the entry and exit of the Pt foil. For the average atom momentum (see above), this probability is found to be

$$P_{br}^{tot}(Pt) = 0.035 \pm 0.001. \quad (3)$$

TABLE I. Summed (over l and m) populations of long-lived atomic states versus n . The populations at the Be target exit and at the Pt foil entry are given in % of the total number of produced $A_{2\pi}$. $P_{br}^{Pt}(np)$ is the breakup probability of the $A_{2\pi} np$ states in the 2.1 μm thick Pt foil. The values are calculated for the average atom momentum 4.44 GeV/c and the ground state lifetime $\tau = 3.15 \times 10^{-15}$ s.

n	2	3	4	5	6	7	8
Be	2.38	1.56	0.85	0.49	0.30	0.20	0.13
Pt	0.48	1.10	0.76	0.47	0.30	0.19	0.13
$P_{br}^{Pt}(np)$	0.763	0.933	0.978	0.991	0.996	0.998	0.999

Number of atoms produced in the Be target.—The analysis of $\pi^+\pi^-$ experimental data, produced in the Be target, is similar to the $\pi^+\pi^-$ analysis as presented in Ref. [3]. The main difference is a shift in Q_Y by 13.1 MeV/c, due to the magnetic field of the inserted permanent magnet. For the analysis in the current section, the found Q_Y value of each experimental and MC event is lessened by the above 13.1 MeV/c.

Events with transverse $Q_T < 4$ MeV/c and longitudinal $|Q_L| < 15$ MeV/c are selected to be analyzed. The experimental Q distribution $N(Q_i)$ and the distributions of its projections are fitted by simulated distributions of atomic $n_A^{MC}(Q_i)$, Coulomb $N_C^{MC}(Q_i)$, and non-Coulomb $N_{nC}^{MC}(Q_i)$ pairs. The numbers of atomic (n_A), Coulomb (N_C), and non-Coulomb (N_{nC}) pairs are free fit parameters in the χ^2 minimization. The sum of these parameters is equal to the number of analyzed events. The fitting procedure takes into account the statistical errors of the experimental distributions.

Table II summarizes the number of Coulomb pairs N_C from the one-dimensional Q and $|Q_L|$ analyses and from the two-dimensional $(|Q_L|, Q_T)$ analysis. The efficiency of Coulomb pair recording is evaluated from the simulated data as ratio of the MC Coulomb pair number N_C^{MC} , passing the corresponding cuts—in each of the above analyses—to the full number of generated Coulomb pairs $N_C^{MC}(0)$: $\epsilon_C = N_C^{MC}/N_C^{MC}(0)$. The full number of produced Coulomb pairs in the Be target is then given by N_C/ϵ_C . This number allows us to calculate the number N_A of atoms produced in the Be target: using the theoretical ratio $K = N_A/N_C$ [Eq. (2)], calculated for $q \leq 2$ MeV/c, and the

TABLE II. Number N_C of Coulomb pairs from different analyses and fit quality as χ^2/n (n is degree of freedom). N_A is the corresponding number of atoms produced in the Be target and N_A^{tot} the total number of atoms after correction for the coplanarity cut. The errors are statistical ones.

Analysis	N_C	χ^2/n	N_A	N_A^{tot}
Q	321 340 \pm 2660	33/27	12 539 \pm 97	17 000 \pm 130
$ Q_L $	315 830 \pm 3250	30/27	12 320 \pm 120	16 700 \pm 160
$ Q_L , Q_T$	319 890 \pm 2610	152/117	12 483 \pm 97	16 960 \pm 130

simulated probability $\epsilon_K = N_C^{MC}(K)/N_C^{MC}(0)$, that the Coulomb pairs have momenta $q \leq 2$ MeV/c, results in $N_A = K\epsilon_K N_C/\epsilon_C$. To recover the losses due to the coplanarity cut in the trigger system, the number N_A is additionally corrected (MC). The corrected values N_A^{tot} are shown in the last column of Table II.

Number of long-lived atoms broken up in Pt.—Atomic pairs from the $A_{2\pi}^L$ atom breakup in the Pt foil are observed [18] above background $\pi^+\pi^-$ pairs produced mainly in the Be target. For the analysis, the same approach is applied as in the previous section, but this time Q_Y is shifted by 2.3 MeV/c for all pairs instead of 13.1 MeV/c (Fig. 1).

In the two-dimensional $(|Q_L|, Q_T)$ analysis, experimental data are analyzed by means of corresponding simulated distributions. For $|Q_L| < 15$ MeV/c and $Q_T < 2$ MeV/c, the $|Q_L|$ projection of the experimental two-dimensional distribution as well as of the three types of simulated $\pi^+\pi^-$ pairs is shown in Fig. 5(a). One observes an excess of events—above the sum of Coulomb and non-Coulomb pairs—in the low Q_L region, where atomic pairs are expected. After background subtraction, there is a statistically significant signal of $n_A^L = 436 \pm 57$ as presented in Fig. 5(b). The signal shape is compared with the simulated distribution of atomic pairs resulting from the $A_{2\pi}^L$ breakup in the Pt foil. The description is acceptable in

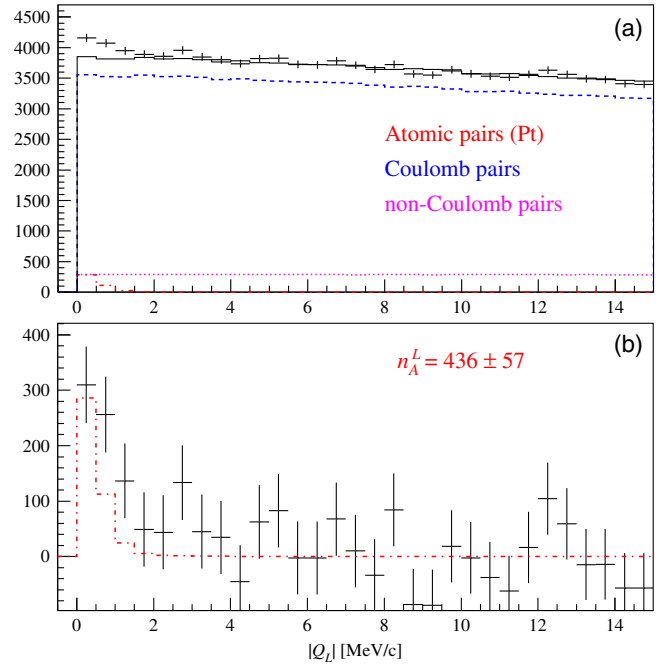


FIG. 5. $|Q_L|$ distribution of $\pi^+\pi^-$ pairs for $Q_T < 2.0$ MeV/c. Plot (a) presents the experimental distribution (+ with statistical error bar) and the simulated background (solid line). Plot (b) shows the experimental distribution after background subtraction (+ with statistical error bar) and the simulated distribution of atomic pairs from $A_{2\pi}^L$ broken up in Pt (dotted-dashed line). The fit procedure has been applied to the two-dimensional $(|Q_L|, Q_T)$ distribution.

view of large statistical uncertainties induced by subtracting two large numbers in the bins of the signal distribution (discussion below).

The Λ width correction accuracy (second section) leads to a systematic error in n_A^L of $\sigma_A^{\text{sys}} = 4.4$. The accuracy of the measured Pt foil thickness causes a systematic error of $\sigma_{P_t}^{\text{sys}} = 22$ in the two-dimensional analysis. Generation of $\pi^+\pi^-$ pairs by beam halo protons is negligible [18].

An additional one-dimensional $|Q_L|$ analysis is performed to check the influence of the simulated atomic pair shape. The experimental distribution is analyzed with three free parameters (fractions of atomic, Coulomb, and non-Coulomb pairs) in the range $0 < |Q_L| < 15$ MeV/ c , and with two parameters (fractions of Coulomb and non-Coulomb pairs) in the interval $2 < |Q_L| < 15$ MeV/ c , where no atomic pairs are expected. In the region $|Q_L| < 2$, $Q_T < 4$ MeV/ c , the atomic pair numbers obtained with the three-parameter fit are $n_A^L = 435 \pm 103$ and obtained with the two-parameter fit $n_A^L = 579 \pm 164$. The difference in n_A^L is mainly due to different signal shapes in the experiment and simulation and is taken as an estimate for the systematic error (only with positive sign) $\sigma_{\text{shape}}^{\text{sys}} = 144$. The systematic error of the number of atoms produced in Be (N_A^{tot}) is calculated as a maximum difference between the value of the analysis with the current variables and other analyses, $\sigma_A^{\text{sys}} = 260$.

In summary, the analysis of the two-dimensional ($|Q_L|$, Q_T) distributions yields the following value for the total probability that a $\pi^+\pi^-$ atom produced in Be breaks up in the Pt foil:

$$P_{\text{br}}^{\text{tot}}(\text{Pt}) = \frac{n_A^L}{N_A^{\text{tot}}} = 0.0257 \pm 0.0034 \Big|_{\text{stat}}^{+0.0086} \Big|_{\text{syst}}^{-0.0014} = 0.0257_{-0.0036}^{+0.0092} \Big|_{\text{tot}}. \quad (4)$$

This result agrees within errors with $P_{\text{br}}^{\text{tot}}(\text{Pt})$ from Eq. (3) calculated by means of QED lifetimes of long-lived states.

Measuring a long-lived $\pi^+\pi^-$ atom lifetime.—A long-lived atom lifetime is evaluated by means of two analyses. In the first simplified analysis, all long-lived atoms are considered as objects, which have one common lifetime, the average momentum $\langle P_A \rangle$ and the breakup probability in the Pt foil equal to 1. The long-lived atom lifetime estimated in this way is

$$\tau = (2.32 \pm 0.35) \Big|_{\text{stat}}^{+0.90} \Big|_{\text{syst}}^{-0.15} \times 10^{-11} \text{ s} = (2.32_{-0.38}^{+0.96}) \Big|_{\text{tot}} \times 10^{-11} \text{ s}.$$

This value of the long-lived atom lifetime is more than three orders of magnitude larger than our measured value of the atom ground state lifetime $\tau_{1s} = (3.15_{-0.26}^{+0.28}) \times 10^{-15} \text{ s}$ [3]. Accounting for the additional calculation errors,

discussed in the ‘‘Population of long-lived states’’ subsection, leads to almost the same value: $\tau = (2.33_{-0.39}^{+0.98}) \times 10^{-11} \text{ s}$.

In the second more sophisticated analysis, the populations of the pionium states are described in terms of transport equations for the whole path from the production point in the Be target to the exit of the Pt foil. For the gap between Be and Pt, radiation transition rates and annihilation of short-lived states are included in the transport equations. The variation of the different $A_{2\pi}^L$ lifetimes τ_{nl} from their QED values τ_{nl}^{QED} [15] is done via the factor $\alpha = \tau_{nl}/\tau_{nl}^{\text{QED}}$, which is the same for any nl level. All the probabilities involved in these calculations are averaged over the spectrum of the observed atoms.

The solid line curve in Fig. 6 presents the breakup probability $P_{\text{br}}^{\text{tot}}(\text{Pt})$ [see Eq. (3)] as a function of the factor α . The error band (dashed curves) accounts for the different extrapolations of the state population for $n \geq 10$. The horizontal lines are the measured value $P_{\text{br}}^{\text{tot}}(\text{Pt})$ together with the total errors [Eq. (4)]. This value corresponds to $\alpha = 0.376_{-0.183}^{+0.804}$. As $\alpha = 1$ is included in the error band, one concludes that the measured lifetime does not contradict the QED calculations. The lifetime of the $2p$ state, which is the shortest-lived of all long-lived states, is found to be $\tau_{2p} = (0.44_{-0.21}^{+0.94}) \times 10^{-11} \text{ s}$. This value is in agreement with the calculation in QED, $\tau_{2p} = 1.17 \times 10^{-11} \text{ s}$ [15].

Accounting for the additional calculation errors, discussed in the ‘‘Population of long-lived states’’ subsection, leads to a wider error band for $\alpha = 0.383_{-0.254}^{+0.926}$, leaving the central value practically unchanged, and to the $2p$ lifetime τ_{2p} :

$$\tau_{2p} = (0.45_{-0.30}^{+1.08}) \times 10^{-11} \text{ s}. \quad (5)$$

The magnetic field between the Be target and the Pt foil transforms into an electric field in the atom c.m. system. This

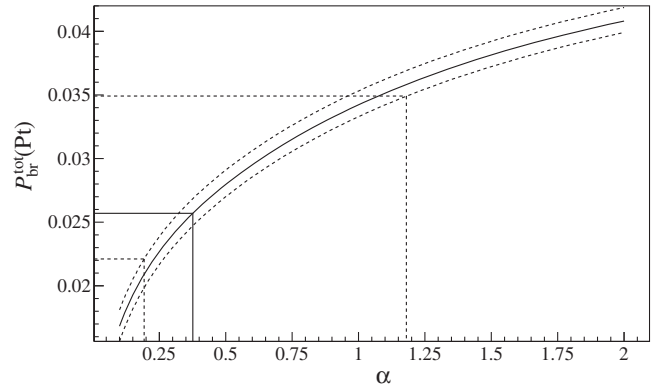


FIG. 6. Probability $P_{\text{br}}^{\text{tot}}(\text{Pt})$ calculated as a function of α (see text). The horizontal lines correspond to the measured value $P_{\text{br}}^{\text{tot}}(\text{Pt}) = 0.0257_{-0.0036}^{+0.0097} \Big|_{\text{tot}}$ [Eq. (4)] together with the total errors. The value $\alpha = 1$, which corresponds to pure QED calculations, is within the error band of the measurement.

field mixes the wave functions of long-lived np states and short-lived ns states resulting in shortening the observed lifetime of np states. The influence of the magnetic field on the lifetime for $2p$ and $2s$ states has been evaluated in Ref. [16]. The magnetic field in the gap shortens the $2p$ lifetime by 1.002 and even more for higher n . To estimate a maximum reduction, all np states with $n > 3$, around 8.6% of all long-lived states at the Be exit, have been considered as decayed in the gap. In this extreme case, the value of the $2p$ lifetime is $\tau_{2p} = (0.60^{+1.34}_{-0.30}|_{\text{tot}}) \times 10^{-11}$ s, not contradicting the result in Eq. (5), evaluated without taking into account the influence of the magnetic field.

Conclusion.—The evaluated lifetime $\tau_{2p} = (0.45^{+1.08}_{-0.30}|_{\text{tot}}) \times 10^{-11}$ s is three orders of magnitude larger than our previously measured value of the $A_{2\pi}$ ground state lifetime $\tau = (3.15^{+0.28}_{-0.26}|_{\text{tot}}) \times 10^{-15}$ s [3]. To consolidate this investigation, the study of $\pi^+\pi^-$ atoms with long-living states should be continued. The outcome opens a possibility to measure the *Lamb shift* of this atom and, herewith, a new $\pi\pi$ scattering length combination $2a_0 + a_2$. These scattering lengths have been calculated in the framework of Chiral perturbation theory and are nowadays investigated in lattice QCD.

We are grateful to O. V. Teryaev for the useful discussions; A. Vorozhtsov, D. Tommasini, and their colleagues from TE-MS/CERN for the Sm-Co magnet design and construction; R. Steerenberg and the CERN-PS crew for the delivery of a high quality proton beam and the permanent effort to improve the beam characteristics. The project DIRAC has been supported by CERN, the JINR administration, the Ministry of Education and Youth of the Czech Republic by Project No. LG130131, the Istituto Nazionale di Fisica Nucleare and the University of Messina (Italy), the Grant-in-Aid for Scientific Research from the Japan Society for the Promotion of Science, the Ministry of Research and Innovation (Romania), the Ministry of Education and Science of the Russian Federation and Russian Foundation for Basic Research, the Dirección Xeral de Investigación, Desenvolvemento e Innovación, Xunta de Galicia (Spain), and the Swiss National Science Foundation.

*Corresponding author.
Juerg.Schacher@cern.ch
†Deceased.

[1] L. Afanasyev *et al.*, *Phys. Lett. B* **308**, 200 (1993).

- [2] B. Adeva *et al.*, *Phys. Lett. B* **619**, 50 (2005).
 [3] B. Adeva *et al.*, *Phys. Lett. B* **704**, 24 (2011).
 [4] B. Adeva *et al.*, *Phys. Lett. B* **674**, 11 (2009).
 [5] B. Adeva *et al.*, *Phys. Lett. B* **735**, 288 (2014).
 [6] B. Adeva *et al.*, *Phys. Rev. Lett.* **117**, 112001 (2016).
 [7] B. Adeva *et al.*, *Phys. Rev. D* **96**, 052002 (2017).
 [8] L. Nemenov, *Yad. Fiz.* **41**, 980 (1985) [*Sov. J. Nucl. Phys.* **41**, 629 (1985)].
 [9] J. Uretsky and J. Palfrey, *Phys. Rev.* **121**, 1798 (1961).
 [10] S. M. Bilenky *et al.*, *Yad. Phys.* **10**, 812 (1969) [*Sov. J. Nucl. Phys.* **10**, 469 (1969)].
 [11] H. Jallouli and H. Sazdjian, *Phys. Rev. D* **58**, 014011 (1998); **58**, 099901(E) (1998).
 [12] M. A. Ivanov, V. E. Lyubovitskij, E. Z. Lipartia, and A. G. Rusetsky, *Phys. Rev. D* **58**, 094024 (1998).
 [13] J. Gasser, V. E. Lyubovitskij, A. Rusetsky, and A. Gall, *Phys. Rev. D* **64**, 016008 (2001).
 [14] G. Colangelo, J. Gasser, and H. Leutwyler, *Nucl. Phys.* **B603**, 125 (2001).
 [15] V. D. Ovsyannikov, CERN, Report No. DIRAC-note-2015-01, <https://cds.cern.ch/record/2012229>.
 [16] L. Nemenov and V. D. Ovsyannikov, *Phys. Lett. B* **514**, 247 (2001).
 [17] L. Nemenov, V. D. Ovsyannikov, and E. V. Chaplygin, *Nucl. Phys.* **A710**, 303 (2002).
 [18] B. Adeva *et al.*, *Phys. Lett. B* **751**, 12 (2015).
 [19] B. Adeva *et al.*, CERN, Report No. CERN-SPSC-2011-001, <https://cds.cern.ch/record/1319290>.
 [20] A. Vorozhtsov *et al.*, CERN, Report No. DIRAC-note-2013-04, <https://cds.cern.ch/record/1622178>.
 [21] B. Adeva *et al.*, *Nucl. Instrum. Methods Phys. Res., Sect. A* **839**, 52 (2016).
 [22] A. Benelli and V. Yazkov, CERN, Report No. DIRAC-note-2013-03, <https://cds.cern.ch/record/1622175>.
 [23] G. Gamov, *Z. Phys.* **51**, 204 (1928).
 [24] A. Sommerfeld, *Atombau und Spektrallinien* (F. Vieweg & Sohn, Braunschweig, 1931).
 [25] A. D. Sakharov, *Sov. Phys. Usp.* **34**, 375 (1991).
 [26] L. Afanasyev and O. Voskresenskaya, *Phys. Lett. B* **453**, 302 (1999).
 [27] L. G. Afanasyev and A. V. Tarasov, *Yad. Fiz.* **59**, 2212 (1996); *Phys. At. Nucl.* **59**, 2130 (1996).
 [28] L. Afanasyev, C. Santamarina, A. Tarasov, and O. Voskresenskaya, *J. Phys. B* **37**, 4749 (2004).
 [29] B. Adeva *et al.*, CERN, Report No. CERN-EP-2018-281, <https://cds.cern.ch/record/2642499>.
 [30] T. A. Heim, K. Hencken, D. Trautmann, and G. Baur, *J. Phys. B* **33**, 3583 (2000).
 [31] T. A. Heim, K. Hencken, D. Trautmann, and G. Baur, *J. Phys. B* **34**, 3763 (2001).
 [32] M. Schumann, T. Heim, K. Hencken, D. Trautmann, and G. Baur, *J. Phys. B* **35**, 2683 (2002).